Effect of pore size polydispersity on the acoustic properties of high-porosity solid foams

C T Nguyen, V. Langlois, Johann Guilleminot, Arnaud Duval, Camille Perrot

Effect of Pore size Polydispersity on the Acoustic Properties of High-Porosity Solid Foams

C. T. Nguyen,[1, a)] V. Langlois,[2, b)] J. Guilleminot,[3, c)] A. Duval,[4, d)] and C. Perrot[1, e)]

[1)] *MSME, Univ Gustave Eiffel, CNRS UMR 8208, Univ Paris Est Creteil, F-77454 Marne-la-Vallée, France*

[2)] *Navier, Univ Gustave Eiffel, ENPC, CNRS, F-77447 Marne-la-Vallée, France*

[3)] *Department of Civil and Environmental Engineering, Pratt School of Engineering, Duke University, P.O. Box 90287, 121 Hudson Hall, Durham, North Carolina 27708-0287, USA*

[4)] *Trèves products, services and innovation, 2-4 rue Emile Arquès, CS 70017, 51686 Reims Cedex 2, France*

(Dated: 9 March 2024)

This study investigates the influence of pore size polydispersity on the acoustic behavior of high-porosity solid foams, using numerical simulations. The effect of the size of the periodic unit cell (PUC) on the transport parameters is first examined. It is found that the size of the PUC required for properly estimating the acoustic properties of random foams depends on both the analyzed transport parameter(s) and level of polydispersity. Assuming identical and constant aperture ratio of membranes, the results indicate that *(i)* the viscous permeability is a reliable indicator regarding the size of the PUC (a more constraining property than the other transport parameters), and *(ii)* high-polydispersity foams require a larger number of pores in the PUC to achieve convergence with respect to morphological characteristics and acoustic properties. The influence of polydispersity on dimensionless transport parameters is then analyzed. It is found that polydispersity has a negligible effect on the high-frequency tortuosity, but induces substantial variations in the remaining macroscopic parameters. Simulations further show that the ratio of the dimensionless transport parameters does not depend on membrane aperture ratio. This important result allows us to propose a fast method to estimate the acoustic properties of a random foam from the transport parameters of monodisperse foams with different pore sizes, for each studied transport parameter. The proposed method is finally employed to characterize the pore size and polydispersity in two real foams (with and without membranes), solving an inverse problem.

[a)]Corresponding author: cong-truc.nguyen@univ-eiffel.fr
[b)]vincent.langlois@univ-eiffel.fr
[c)]johann.guilleminot@duke.edu
[d)]arnaud.duval@treves-group.com
[e)]camille.perrot@univ-eiffel.fr

I. INTRODUCTION

Real foams usually have a disordered structure with a continuous pore-size distribution (polydispersity). They are widely used in various applications requiring sound absorption, noise reduction, thermal insulation, and vibration damping[1,2]. Foams exhibiting high porosity are of significant interest in the automotive and building industries due to their lightweight nature (low density) and excellent acoustic performance. The acoustical properties of rigid foams can be characterized by the so-called Johnson-Champoux-Allard-Lafarge (JCAL) model [3–7]. The latter depends on six input parameters, namely (1) the Darcy static permeability k_0; (2) the high-frequency tortuosity α_∞; (3) the viscous characteristic length Λ; (4) the static thermal permeability k_0'; (5) the thermal characteristic length Λ'; and (6) the open porosity ϕ. These macroscopic parameters depend on the microstructure, which is characterized by parameters such as pore size and shape, membrane content, and ligament cross-section for open-cell foams without membranes.

The effect of the microstructural parameters on macroscopic acoustic properties has been examined, either computationally or experimentally, in several works. For example, the impact of pore average size and closed membranes was studied with a semi-empirical approach by Doutres *et al.*[8,9]. Hoang *et al.*[10] investigated the effect of the membrane aperture degree. Foams having both partially open and closed membranes were considered in the works of Gao *et al.*[11] and Trinh *et al.*[12]. While these previous studies have primarily focused on the impact of pore average size, the effect of polydispersity has received much less attention to date. This is mostly due to the prohibitive computational cost required to solve boundary value problems on large spatial domains.

Previous studies focusing on either the elastic behavior[13,14] or the permeability[15,16] of polydisperse foam have recently been published. However, none of these research works addressed the diversity of transport properties collectively. To the authors' best knowledge, there is only one analytical model, developed by Horoshenkov *et al.*, that can relate polydispersity to the six transport parameters in the JCAL model[6,7,17,18]. However, no validation with either experimental measures or numerical simulations has been undertaken so far. In a previous publication, Langlois *et al.* has investigated the permeability of solid foams with variations in the pore size distribution[15]. More recently, a multi-scale approach was developed to establish a link between the microstructure of a polydisperse foam and its acoustical

properties[19]. This model relies on Laguerre tessellation to generate periodic unit cells, and simplified models were proposed to reduce the computational cost (including a pore-network approach to estimate the viscous permeability). In this study, the pore size distribution was taken into account through the geometrical proxy, and the effect of polydispersity on the acoustic properties of a real high-porosity PU foam was analyzed. The goal of this work is twofold. First, we aim to provide a comprehensive study of the effect of polydispersity on all transport parameters. Second, we seek to assess the predictive capabilities of Horoshenkov's model.

The paper is organized as follows. Section II presents the generalization of PUCs for random foams and the simulation method used to obtain macroscopic properties. Section III discusses the effect of PUC size on the acoustic properties, followed by a study on the impact of pore size polydispersity based on the REV determined from the PUC size study. This section also proposes a fast method to simulate the acoustical behavior of random foams. In Section IV), we leverage the proposed approach and introduce a methodology to identify, through an inverse problem, the pore size polydispersity and membrane content. This identification process is then applied to analyze the microstructure of two real foams. Finally, Section V provides concluding remarks.

II. THEORY AND METHODOLOGY

The aim of this section is to provide a brief overview of the procedure. Interested readers are referred to[19] for a detailed description and validation on a real polydisperse PU foam.

A. PUC Microstructure Generation

The numerical determination of the acoustic properties requires the reconstruction of periodic unit cells. Two microstructure parameters are considered: *(i)* the pore diameter, denoted by d_p; and *(ii)* the sphericity, denoted by ψ. The former is defined as the diameter of a sphere having the same volume (V_p) as the actual, and potentially non-spherical, pore. The latter is defined as the ratio of the surface area of a sphere having the same volume as the pore, to the surface area (S_p) of the pore: $\psi = (36\pi)^{1/3} V_p^{2/3}/S_p$. The level of polydispersity

in a random foam is then measured by the coefficient of variation of the pore size:

$$C_d = \frac{\sigma_d}{d}, \tag{1}$$

where d is the pore number-weighted size average and σ_d is the corresponding standard deviation. In this work, PUC microstructures are generated using Neper software[20]. A

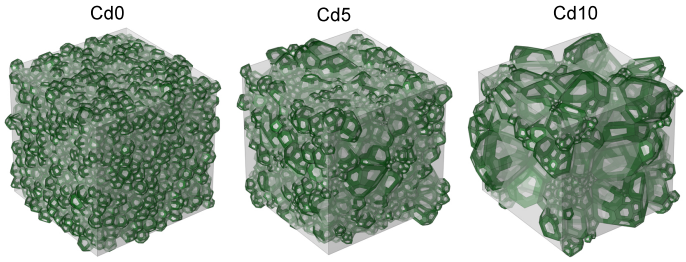

FIG. 1. Samples of PUC microstructures. The PUC size is normalized by pore size average, $L/d = 10$.

log-normal distribution is assumed for the pore size and the asphericty variable $(1 - \psi)$, interpreted as a shape parameter, is used as an additional input. In accordance with the multiscale setting (to be described momentarily), periodic boundary conditions are applied in all directions.

To study the effect of pore size variations, PUCs are generated with increasing levels of polydispersity, keeping the average pore size d constant. All membranes are open with an identical aperture ratio defined as $\tau_o = \sqrt{S_o/S_w}$, where S_o is the area of the membrane aperture and S_w is the total area of the membrane (see Sec. 2.2 of Ref.[19] for details regarding practical implementation). The sphericity ψ is maximized for each value of C_d. As shown in[21], the structure of a random foam obtained by minimizing the surface area gives maximal sphericity. However, this relaxation process is very time-consuming and remains challenging for large polydispersity levels. Laguerre structures with maximal sphericity, on the other hand, provides a cheaper alternative and were shown to deliver comparable permeability predictions in the case of constant aperture ratios[15]. Note that the tessellation typically includes numerous small faces. Although these components have a negligible impact on the morphology of the cells, they may compromise the stability of a foam structure[22]. Consequently, small faces are disregarded during the opening procedure when the condition

$S_w \leq 10^{-4}d^2$ is satisfied. The polydispersity levels obtained following this procedure are given in Tab. I. Samples of the foam microstructure associated with three levels of polydispersity are shown in Fig. 1. Here, the PUC size L is normalized by the pore size average, $L/d = 10$. In the procedure described above, one assumes that the opening ratio τ_o of the membranes is uniformly constant and independent of the polydispersity C_d.

TABLE I. Estimated polydispersity levels in the generated PUC microstructures.

Name	Cd0	Cd1	Cd2	Cd3	Cd4	Cd5	Cd6	Cd7	Cd8	Cd9	Cd10
C_d	0.030	0.107	0.198	0.285	0.366	0.440	0.511	0.574	0.646	0.689	0.730

B. Determination of Transport Parameters

In this section, a brief overview of the boundary value problems (BVPs) that must be solved to estimate the macroscopic properties entering the JCAL model is provided for the sake of self-containedness. This semi-phenomenological model relies on two parameters (ϕ and Λ') that solely depend on the geometry of the microstructure:

$$\phi = \int_{\Omega_f} dV \Big/ \int_{\Omega} dV \ , \quad \Lambda' = 2 \int_{\Omega_f} dV \Big/ \int_{\partial\Omega} dS \ , \tag{2}$$

where Ω is the solid boundary, Ω_f is the volume occupied by the fluid, and $\partial\Omega$ represents the solid border. The remaining transport properties are computed using the solutions to three BVPs formulated on the PUC, detailed below.

- **BVP-1**: The low-Reynolds flow of an incompressible Newtonian fluid is governed by the Stokes equations in the fluid phase:

$$\mu \boldsymbol{\Delta} \mathbf{v} - \nabla p = -\nabla p \quad \text{in} \quad \Omega_f \ , \tag{3}$$

$$\nabla . \mathbf{v} = 0 \quad \text{in} \quad \Omega_f \ , \tag{4}$$

$$\mathbf{v} = 0 \quad \text{on} \quad \partial\Omega \ , \tag{5}$$

  where $\mathbf{v}$, p, and μ are the velocity, pressure, and viscosity of the fluid, respectively. Here, $\mathbf{v}$ and p are L-periodic. The term ∇p is a macroscopic pressure gradient acting as a forcing term. The macroscopic pressure gradient λ_m is defined as $\lambda_m = \Delta p / L$.

The static viscous permeability k_0 is calculated using the average of the microscopic velocity over the pore fluid volume, denoted by $\langle \mathbf{v} \rangle$:

$$k_0 = \mu \frac{\langle \mathbf{v} \rangle \cdot \mathbf{e}}{\lambda_m} \,, \tag{6}$$

where $\mathbf{e}$ is the unit vector pointing in the direction of the macroscopic pressure gradient. We note that because most of the pressure drop is indeed located in the vicinity of the membrane aperture, a simplified calculation of the fluid flow based on a pore-network hypothesis is possible, building upon the foundation established by Koplik (1981)[23] and later developments by Langlois *et al.* for monodisperse and polydisperse foams[15,24].

- **BVP-2**. In the high frequency range, the influence of the viscous boundary layer diminishes, and the fluid behaves as a perfect or inviscid fluid, flowing through the pore space in a manner analogous to the migration of electric charges in a conducting fluid of constant conductivity. Thus, the fluid behavior can be described as an electrical conduction problem[3,25]:

$$\nabla \cdot \mathbf{E} = 0 \quad \text{in} \quad \Omega_f \,, \tag{7}$$

$$\mathbf{E} = -\nabla\varphi + \mathbf{e} \quad \text{in} \quad \Omega_f \,, \tag{8}$$

$$\mathbf{E} \cdot \mathbf{n} = 0 \quad \text{on} \quad \partial\Omega \,, \tag{9}$$

where $\mathbf{E}$ is the solution exhibiting $-\nabla\varphi$ as a fluctuating component, φ is L-periodic, and $\mathbf{n}$ is the outward-pointing unit normal to the boundary of the pore region. The high-frequency tortuosity α_∞ and viscous characteristic length Λ are then calculated as:

$$\Lambda = \frac{2\int_{\Omega_f} \mathbf{E}^2 dV}{\int_{\partial\Omega} \mathbf{E}^2 dS} \,, \quad \alpha_\infty = \frac{\langle \mathbf{E}^2 \rangle}{\langle \mathbf{E} \rangle^2} \,. \tag{10}$$

It should be noted that due to the presence of a sharp edge near the membrane apertures, the electric field exhibits a singularity along this edge. To accurately resolve the field, the element size h was locally refined along the aperture edge. In practice, this size corresponds to the thickness of the membranes and was set to $h = d/1000$, given our focus on thin membrane foams. Further details can be found in Appendix A of Ref.[19].

- **BVP-3**. When excited by a harmonic external source, a uniform harmonic heating in the air domain results in an excess temperature field, with perfect absorbing conditions on the solid boundaries. The static thermal permeability can be then determined as[5]:

$$k_0' = \phi\langle u\rangle \ , \tag{11}$$

in which the L-periodic temperature field u is the solution to the Poisson equation, supplemented with the thermostat boundary condition:

$$\Delta u = -1 \quad \text{in} \quad \Omega_f \ , \tag{12}$$

$$u = 0 \quad \text{on} \quad \partial\Omega \ . \tag{13}$$

To solve BVP-2 et BVP-3, the finite element method is used (Sec. 2.3 of Ref.[19]). It should be noticed that microstructure randomness induces stochasticity in the above estimates. In this case, overall effective transport parameters can be determined using averages over orientations (here, the three directions defined by the Cartesian axes in the PUC). Note that, due to the homothety of the generated PUC structures and in accordance with the scaling rules[26], the transport parameters $\mathcal{TP}$ of a foam structure with the average pore diameter d can be described in the form of normalized (dimensionless) quantities $\mathcal{TP}^*$: $k_0^* = k_0/d^2$; $k_0'^* = k_0'/d^2$; $\Lambda^* = \Lambda/d$; $\Lambda'^* = \Lambda'/d$ and $\alpha_\infty^* = \alpha_\infty$. More specifically, the *dimensionless* or *normalized* transport parameters represent the values obtained from the PUC structures in which the average pore size is set to one. Furthermore, the membranes of PUC structures generated in Sec. II A have no thickness, implying that $\phi = 1$.

III. RESULTS AND DISCUSSIONS

A. On the Size of the Periodic Unit Cell

In this section, we aim to determine the size of the representative volume element by assessing the convergence of transport parameters with respect to the size of the periodic unit cell L, normalized by the average pore size d. Fig. 2 shows the evolution of the mean and standard deviation of each dimensionless transport parameter as a function of the domain size L/d for three types of foams (Cd0, Cd5, and Cd10). The statistical values corresponding to each domain size are obtained from 5 microstructure realizations (results averaged over

the three principal directions). The latter type of foams are ordered according to increasing polydispersity.

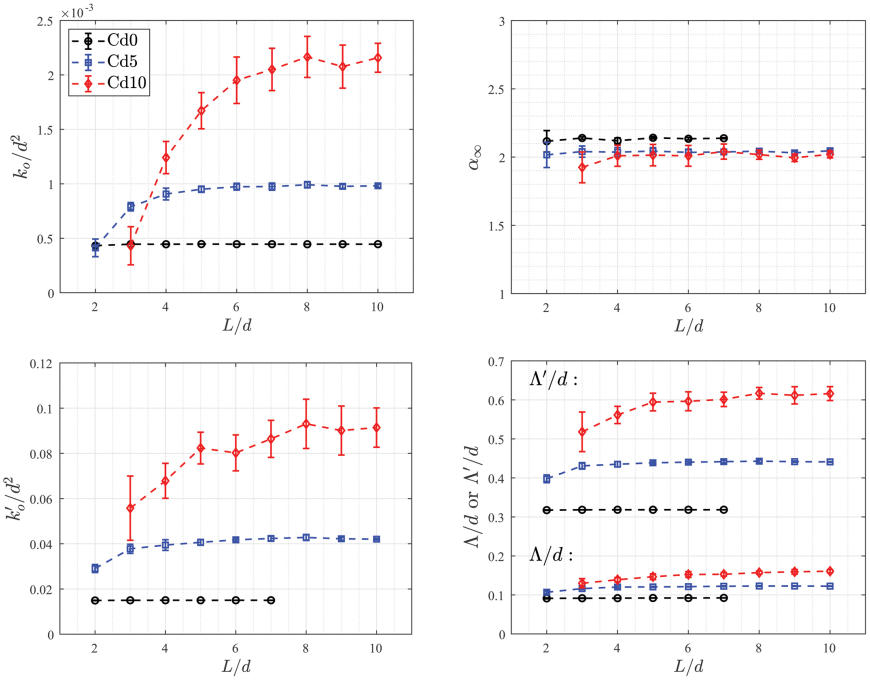

FIG. 2. Evolution of dimensionless transport parameters as a function of L/d. Membrane aperture ratio is set to $\tau_o = 0.25$. Error bars indicate standard deviations.

As expected, a convergence in mean and a reduction in variance is observed as L/d increases. This is because the size of the PUC also increases with the number of pores within it, which implies statistical convergence for the morphological characteristics. The convergence of some morphological characteristics is shown in Fig. 3, including the polydispersity C_d and the coefficient of variation of the membrane surface CV_S (defined as the ratio between the standard deviation σ_S and the average S of the membrane surface). While C_d measures the variation in pore size, CV_S quantifies the dispersion in the interconnection size between pores in the foam microstructure. Indeed, the pore size and the interconnection size are two of the most important morphological properties influencing the acoustical properties[9,11,27]. Although C_d is one implicit input parameter in the microstructure reconstruction proce-

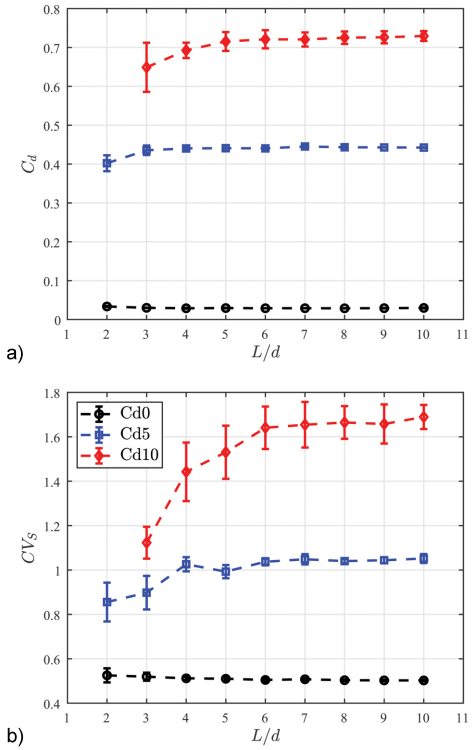

FIG. 3. Evolution of morphology features C_d and CV_S versus normalized size of PUC L/d. The error bars correspond to standard deviations.

dure, it can only achieve a desired value if the size of the PUC is sufficiently large — or the number of pores in the PUC is sufficiently high, as evidenced by the results presented in Fig. 3a. Regarding the interconnection size, it can be observed that CV_S requires a larger size of PUC in order to converge. The similarity observed in the evolution of both CV_S (Fig. 3b) and the transport parameters (Fig. 2) suggests that the convergence of the acoustic properties can be inferred from the convergence of the distribution of interconnection size. Indeed, Langlois *et al.*[15] have suggested that the permeability is proportional to r_o^3, where $r_o = t_o\sqrt{S/\pi}$. Here, r_o denotes the opening radius. The convergence of k_0 is expected to exhibit some dependency with the membrane size as $CV_{S^{1.5}}$ (with $S^{1.5} = \pi^{1.5}\,(r_o/\tau_o)^3$). Similarly, for very small opening ratio, the tortuosity is also expected to exhibit some degree

of dependency with membrane size S as $CV_{S^{0.5}}$ (with $S^{0.5} = \pi^{0.5}\,(r_o/\tau_o)$)[28]. The dependency on r_o^3 and r_o^1 may describe the sensitivity of the transport parameter on the convergence of the microstructure.

The rate at which the acoustic properties of a random foam converges with respect to the PUC size is evidently influenced by polydispersity. A foam with a greater range of pore sizes or greater dispersion in its microstructure necessitates a larger number of pores in the PUC to realize statistical convergence in key morphological characteristics, thereby requiring a PUC with a larger size than a less polydisperse foam. In particular, the properties of a monodisperse foam can be accurately estimated with a normalized PUC size of $L/d = 2$ (15 pores), for a random microstructure, or even $L/d = 1$ (with only 2 pores) if a Kelvin ordered structure is used. On the other hand, the properties of a high polydispersity random foam (such as Cd10) requires a normalized PUC size of $L/d = 10$, which corresponds to 317 pores. Note that the number of pores is determined from the ratio L/d based on the probability density function of a lognormal law describing the pore size distribution; see Eq. 13 of Ref.[20]. The increase of the RVE size with polydispersity, quantified using the permeability and the specific surface area, was noticed in[29] for rock samples (Figs. 11-13 in[29]).

It is important to note that the convergence rate varies across different transport parameters, and this effect is particularly pronounced for foams with high polydispersity. Indeed, a study by Kanit *et al.* (2003)[30] in the context of thermoelasticity demonstrated that the minimum RVE size depends on whether thermal or elastic properties are analyzed. Here, the acoustic properties are determined by transport parameters that are estimated using different boundary value problems (see Section II B). This provides an explanation for the observed discrepancies in terms of convergence rates. Fig. 4 illustrates the variations of the transport parameters as a function of the normalized PUC size L/d for foam Cd10. The transport parameters are normalized based on their corresponding values at $L/d = 10$, which is the point at which all parameters are assumed to be converged. The convergence of all parameters is independent of the aperture ratio τ_o. However, the high-frequency tortuosity α_∞ exhibits a small variation when compared to the other transport parameters, meaning that the influence of the PUC size is smaller on α_∞. Meanwhile, the convergence rate of the permeabilities k_0 and k_0' is slower than the one of the characteristic lengths Λ and Λ'. The observed difference in convergence rates implies that the REV size corresponding to the viscous permeability k_0 is larger than the REV size of the other transport parameters.

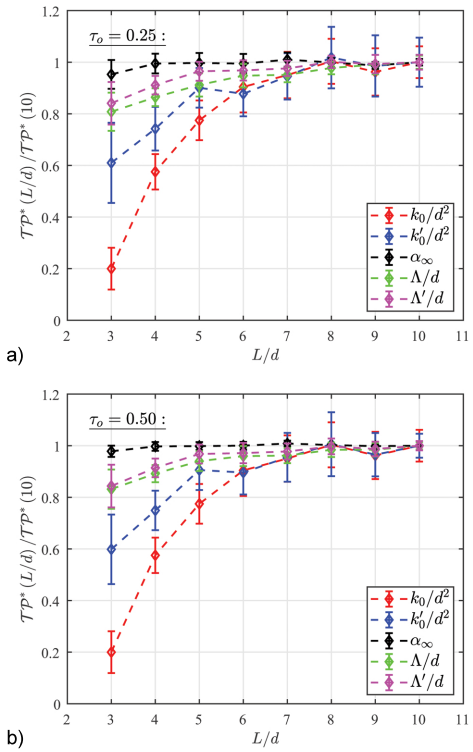

FIG. 4. Convergence of transport parameters for Cd10. The error bars correspond to standard deviations.

As a consequence, having identified the REV size of the viscous permeability means having identified a REV size appropriate for the acoustical properties of a random foam. In Refs.[29,31], it was noted that various realistic porous media corresponding to rock samples exhibit a similar pattern, where the size of the RVE required for flow-related properties (such as viscous permeability k_0) is greater than the size of RVE needed for geometric properties (the thermal characteristic length Λ').

This observation has important practical implications for determining sample sizes in experimental characterization. For instance, analyzing 3D micro-CT images to extract morphological features of a random media can be computationally intensive. Since the viscous permeability k_0 can be computed directly from micro-CT images[29,32], it can be used to de-

termine the minimum sample size required to ensure statistical convergence of morphological parameters. Additionally, a sample size that achieves convergence for the permeability can be considered reliable for characterizing other transport and acoustic properties.

B. Polydispersity Effect and Equivalent Pore Size

In this section, we will focus on how polydispersity affects the acoustic properties of random foams. Once again, the model system we consider is based on an aperture of the membranes described using a constant opening ratio τ_o. A novel parameter called γ is introduced. This parameter is based on the ratio of the normalized transport parameters ($\mathcal{TP}^*$) for a polydispersity of C_d to those of a monodispersity with a very low C_d value (i.e., close to zero):

$$\gamma = \left(\frac{\mathcal{TP}^*\left(C_d, \tau_o\right)}{\mathcal{TP}^*\left(0, \tau_o\right)} \right)^{1/\beta}, \tag{14}$$

where $\beta = 1$ for Λ, Λ' and α_∞; and $\beta = 2$ for k_0 and k_0'. On the one hand, the evolution of γ enables to describe the effect of polydispersity C_d on the acoustic properties of foam materials through transport parameters. On the other hand, the parameter γ allows determining the pore size $D_{\mathcal{TP}}$ of a monodisperse foam for which the studied transport parameter (k_0, k_0', Λ, or Λ) matches exactly with the transport parameter of a polydisperse foam having the average pore size d: $D_{\mathcal{TP}} = \gamma \times d$. For this purpose, β is chosen so that the dimension of the associated parameter is given by a length to the β power. Moreover, our numerical results with several values of the aperture ratio ($\tau_o = 0.25$, 0.5, 0.75) show that τ_o has very little influence on γ. Indeed, when plotting the parameter γ as a function of the polydispersity C_d for different values of the aperture ratio τ_o, the relative variation of the parameters γ are lower than 5%. This statement leads us to consider that, in practice, γ is independent of τ_o.

1. Simulation Results

As shown in Fig. 5a, the *simulated* values of all transport parameters increase as C_d increases, with the exception of α_∞ — which exhibits minimal dependence on C_d. The increase of the viscous permeability has been discussed elsewhere in the literature[15], and can be attributed to a significant increase in mean local conductance. This trend is also

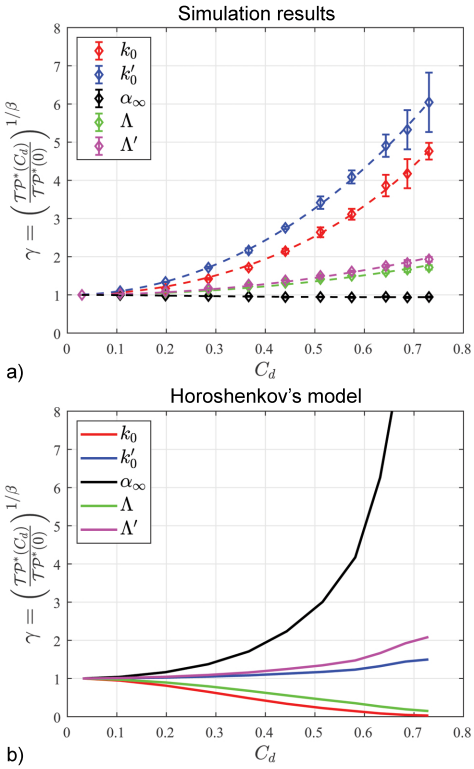

FIG. 5. a) Simulation results ($\tau_o = 0.25$) and b) predictions from Horoshenkov's model. Error bars correspond to standard deviations. In a), dashed lines are plotted from Eqs. (20–24). Note that the outcomes derived from the simulations are unaffected by the membrane aperture ratio τ_o (in the studied range: $0.1 \leq \tau_o \leq 0.9$).

consistent with experimental measurements on open-cell foams without membranes; see[33]. The evolution of the static thermal permeability, k_0', follows a similar pattern as that of k_0. This is because k_0' is a parameter introduced to characterize thermal effects using a thermal equivalent of the dynamic Darcy's law, as explained in[5]. Thus, the static thermal permeability plays a role similar to that of the viscous permeability (although we expect that $k_0' \geq k_0$ and $k_0 \to 0$ when $\tau_o \to 0$, as opposed to k_0'). However, it is noteworthy that the increase of the thermal permeability with respect to polydispersity is more significant than the one observed for the viscous permeability. A plausible explanation for this observation lies in

the fact that a scalar variable (here, the temperature) may be more sensitive to describe microstructural variations in all directions of space than an oriented vectorial variable (here, the mass flux); see Sec. V.D of Ref.[34] for a discussion. Furthermore, it is important to note that an increase in polydispersity results in an increase in the pore volume-to-surface ratio, or in the inverse of the specific surface area (see Fig. 1), as well as in an increase in the viscous and thermal characteristic lengths (denoted by Λ and Λ', respectively). A closer look at the latter quantities reveals that their evolution with C_d is strongly correlated. However, it should be mentioned that the ratio Λ'/Λ is depending on C_d and can not be assumed to be equal to a constant value: the discrepancy between Λ' and Λ increases with C_d.

In the PUC microstructure generation procedure, the aperture ratio τ_o remains constant and we see in Fig. 2 and Fig. 5a that the effect of polydispersity (on the calculated tortuosity) is fairly small, over most of polydispersity range. More specifically, the tortuosity is slightly decreasing with increasing polydispersity (α_∞ slowly decreases by about 5% from Cd0 to Cd10 with $\tau_o = 0.25$). The high-frequency tortuosity α_∞ is influenced by the alteration of fluid velocity in the porous medium, which is in turn connected to the variation of local cross-sectional area (local constriction). In foam materials, the most prominent constrictions are located at the openings of membranes, and hence, the tortuosity is closely related to the aperture ratio τ_o of these membranes. In Ref.[28], it was noted that the tortuosity of solid foam can be driven at the pore level by two types of conductances. The first type is the interpore conductance, which connects two interconnected pores, while the second type is the intrapore conductance, which takes into account the contribution of the pore-filling fluid to total pore conductivity. The interpore conductance depends on the size of the aperture membrane related to τ_o, which is set to a constant value, while the intrapore conductance is related to morphological parameters of the pore space that are relatively independent on C_d[21]. This could explain the almost polydispersity invariance of tortuosity. Indeed, despite the lack of a quantified degree of polydispersity, high-porosity open-cell foams exhibit a constant value of tortuosity ($\alpha_\infty \approx 1.05$) in the literature, including nine fully reticulated polyurethane foams in Ref.[8], foam $P1$ in Ref.[9], foam R_3 in[10,35], and foam sample 5 in Ref.[36]. On the other hand, previous papers by Doutres *et al.*[8,9] indicate that for partially reticulated polyurethane foams, the tortuosity can be empirically estimated as a function of the membrane content (i.e., R_w) alone: $\alpha_\infty = 1.05\,(1/R_w)^{0.3802}$. The validity of this approximation further supports the independence of the tortuosity with respect to

variations in pore size in foam materials.

2. *Comparison With Horoshenkov's Model*

Fig. 5b illustrates the evolution of the transport parameters as predicted by the so-called Horoshenkov's 3-parameter model[17,18]. In the latter, transport parameters of interest are related to the open porosity ϕ and to the parameters defining a log-normal distribution for the pore size (namely, the median pore radius $\bar{s}$, and the standard deviation σ_s in the pore radius distribution taken on the log-normal scale [$-\log_2(s)$ with s denotes the pore radius]) through:

$$\alpha_\infty = e^{4(\sigma_s \log 2)^2}, \tag{15}$$

$$k_0 = \frac{\phi \bar{s}^2}{8\alpha_\infty} e^{6(\sigma_s \log 2)^2}, \tag{16}$$

$$k_0' = \frac{\phi \bar{s}^2}{8\alpha_\infty} e^{-6(\sigma_s \log 2)^2}, \tag{17}$$

$$\Lambda = \bar{s} e^{-5/2(\sigma_s \log 2)^2}, \tag{18}$$

$$\Lambda' = \bar{s} e^{3/2(\sigma_s \log 2)^2}. \tag{19}$$

The results predicted by the analytical models in Eqs. (15)-(19) are in disagreement with the direct numerical simulation results presented above, as well as with the experimental observations obtained for the viscous permeability k_0 reported in Ref.[33] for open-cell foams. This provides an insight about the validity of Horoshenkov's model: while efficient in fitting experimental data for certain types of materials, this model may be inadequate for analyzing foams or cellular materials where the assumption of an infinite sequence of continuous and instantaneous cross-sectional changes — which stands at the core of Horoshenkov's derivations — does not hold. Specifically, the variation of cross-sectional area within the pores is negligible in foam or cellular materials, in which changes primarily occur at the constrictions where pores are connected, or at the level of membrane aperture (if present). As shown in several studies[8–12,19,27,37], the acoustic properties of foams are strongly influenced by membrane content, including the existence of partially- and fully- closed membranes. The inclusion of such morphological features to extend the validity of Horoshenkov's seminal derivations is an interesting problem that is left for future work.

Because the value of γ solely depends on C_d (Fig. 5a), the value of γ for each transport

parameter can be approximated as:

$$\gamma_{\alpha_\infty} = 1, \tag{20}$$

$$\gamma_{k_0} = 5.688\left(e^{0.9548C_d^2} - 1\right) + 1, \tag{21}$$

$$\gamma_{k_0'} = 28.870\left(e^{0.3023C_d^2} - 1\right) + 1, \tag{22}$$

$$\gamma_{\Lambda} = 6.001\left(e^{0.2283C_d^2} - 1\right) + 1, \tag{23}$$

$$\gamma_{\Lambda'} = 9.919\left(e^{0.1757C_d^2} - 1\right) + 1. \tag{24}$$

The coefficient of determination (R-squared) is 0.9985 for γ_{k_0}, 0.9994 for $\gamma_{k_0'}$, 0.9844 for γ_{Λ} and 0.9930 for $\gamma_{\Lambda'}$. These approximations will be used in the next section to develop surrogates models for the transport parameters.

3. Surrogate Models for Transport Parameters

From a practical standpoint, the knowledge of parameter γ (for a given property) and averaged pore size d enables the determination of the transport parameter of a random polydisperse foam based on those of a monodisperse foam through

$$\mathcal{TP}^*\left(C_d\right) = \left(\gamma\right)^\beta \mathcal{TP}^*\left(0\right), \tag{25}$$

according to Eq. (14). It should be noted that the normalized transport parameters of a high-porosity monodisperse foam, $\mathcal{TP}^*\left(0\right)$, only depend on the membrane aperture ratio τ_o. These parameters can be conveniently simulated using the Kelvin unit cell, employing either the finite element method or the pore-network approach. To provide a rapid estimate of these transport parameters without the need for additional simulations, polynomial surrogates can be utilized to establish relationships between the normalized transport parameters and the membrane aperture ratio τ_o of the monodisperse foam. For instance, using the simulation

results on the Kelvin unit cell (see Fig. 6) leads to:

$$\alpha_\infty^*(0) = 497.88\tau_o^6 - 1691.9\tau_o^5 + 2322.2\tau_o^4 - 1649.9\tau_o^3 + 646.21\tau_o^2 - 136.69\tau_o + 14.334, \tag{26}$$

$$k_0^*(0) = 0.0283\tau_o^3, \tag{27}$$

$$k_0'^*(0) = 0.0994\tau_o^3 - 0.0735\tau_o^2 + 0.0242\tau_o + 0.0122, \tag{28}$$

$$\Lambda^*(0) = 31.357\tau_o^5 - 65.618\tau_o^4 + 51.741\tau_o^3 - 18.44\tau_o^2 + 3.1726\tau_o - 0.1573, \tag{29}$$

$$\Lambda'^*(0) = 44.585\tau_o^5 - 93.24\tau_o^4 + 73.568\tau_o^3 - 26.054\tau_o^2 + 4.1708\tau_o + 0.0704. \tag{30}$$

The coefficient of determination (R-squared) is 0.9996 for the tortuosity, 0.9997 for the viscous permeability, 0.9985 for the thermal permeability, 0.9989 for the viscous characteristic length and 0.9987 for the thermal characteristic length. Note that the case $\tau_o = 0$ corresponds to a closed-cell foam where the compressionnal sound wave is reflected without absorption. This case was therefore excluded from the computations, and we restricted our simulations to the range $\tau_o = [0.1 - 0.9]$. For $\tau_o \geq 0.9$ (foam without membrane), the cross-section shape of the ligaments must be taken into account (Fig. 8, Plateau border), and analytical surrogates taking into account the effect of porosity are available in Ref.[38].

Furthermore, the use of the approximations defined by Eqs. (20–24) provides a way to estimate the properties of the corresponding monodisperse/Kelvin pore sizes for a randomly polydisperse foam. An equivalent pore size is described as the pore size in a monodisperse foam or in a Kelvin structure that exhibits the same transport parameter of interest and aperture ratio τ_o as the initial polydisperse foam sample. The scaling law for transport parameters presented in[26,35] utilizes a homothetic transformation and enables the prediction of the acoustic properties of a polydisperse foam by using an equivalent monodisperse foam, characterized by an equivalent pore size:

$$\mathcal{TP}(C_d, d) = (\gamma d)^\beta \mathcal{TP}^*(0) = \mathcal{TP}(0, D_{\mathcal{TP}}), \tag{31}$$

where $D_{\mathcal{TP}} = \gamma d$ represents the pore size of the equivalent monodisperse foam, for each transport parameter. Here, we did not emphasize the dependency of $\mathcal{TP}$ on τ_o in Eq. (31), which is implicit since $\mathcal{TP}^*(0)$ depends on τ_o. Note that the scaling law does not apply to

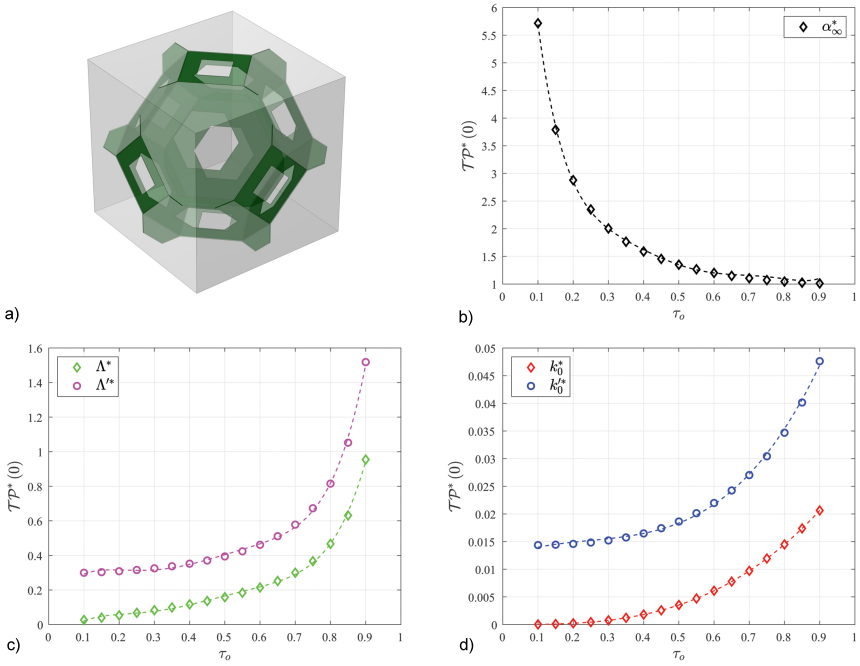

FIG. 6. Dependence of dimensionless transport parameters $\mathcal{TP}^*(0)$ on membrane aperture τ_o of monodiseprse foam modeled by Kelvin unit cell.

the tortuosity α_∞, which is scale-invariant. Therefore, the tortuosity is calculated as:

$$\alpha_\infty(C_d) = \gamma_{\alpha_\infty}\alpha_\infty^*(0). \tag{32}$$

It is important to notice that the equivalent Kelvin pore size does not describe a specific pore representative of all pores in the sample. For example, in the case of a polydisperse sample with a coefficient of variation of pore size equal to 0.73, the pores having a size approximately equivalent to the Kelvin/monodisperse pore size possess an average of around 30 neighboring pores, which is much larger than the expected number of neighbors (around 14) for a Kelvin structure or a typical pore of a monodisperse foam.

Finally, the set of equivalent pore sizes $D_{\mathcal{TP}}$ (for all transport parameters) can also be

employed to assess the reliability of the characterization for the transport parameters, using

$$D_{k_0'} = \left(\frac{k_0'}{k_0'^*(0)}\right)^{0.5} \geq D_{k_0} = \left(\frac{k_0}{k_0^*(0)}\right)^{0.5} \geq D_{\Lambda'} = \frac{\Lambda'}{\Lambda'^*(0)} \geq D_{\Lambda} = \frac{\Lambda}{\Lambda^*(0)}, \tag{33}$$

where $D_{k_0'} = D_{k_0} = D_{\Lambda'} = D_{\Lambda}$ if and only if the foam has uniform pore size[10,11,35]. We note that the larger the differences between the equivalent pore sizes $D_{\mathcal{TP}}$, the larger the pore size dispersion C_d.

IV. INVERSE IDENTIFICATION OF MORPHOLOGICAL CHARACTERISTICS

A detailed description of the micro-geometry of a random foam is very complex because it entails the determination of polydisperse polyhedrons and the characterization of membrane content from advanced imaging techniques (such as X-ray micro computed tomography and scanning electron micrograph images). We assume that characterization techniques are available for the transport parameters at macroscale, including the porosity ϕ[39] and the permeability k_0. The latter can be derived from the characterization of a low-Reynolds fluid flow (to satisfy a purely viscous regime), as specified in the standard ISO 9053-1:2018. The tortuosity α_∞ and the viscous Λ and thermal Λ' characteristic lengths may also be obtained by direct measurements (see[40,41] and[42]). Alternatively, one may solve an inverse problem to identify (α_∞, Λ, Λ', k_0') from the measurements of the real and imaginary parts of the dynamic viscous $k(\omega)$ and thermal $k'(\omega)$ permeabilities, using relevant models[43,44].

In this section, we aim to determine which morphological parameters (characterizing a highly porous random foam) can be identified from the characterization of the transport parameters (ϕ, k_0, α_∞, Λ, Λ', k_0'). Such an inverse problem can be solved by minimizing an adapted cost function (minimizing, e.g., in the L^2 sense, the error between the predicted and measured transport parameters). In the present approach, the identification of the morphological parameters is guided by the knowledge acquired from the previous simulations. The next subsection contains a detailed description of the proposed methodology to identify the membrane aperture ratio τ_o, the averaged pore size d and the pore size polydispersity C_d from the available transport parameters (ϕ, k_0, α_∞, Λ, Λ', k_0').

A. Definition of the Inverse Method

In order to proceed with the inverse identification, the high-porosity assumption must be verified. In practice, we assume that this condition is met when $\phi \geq 0.95$ (Step 1, Fig. 7).

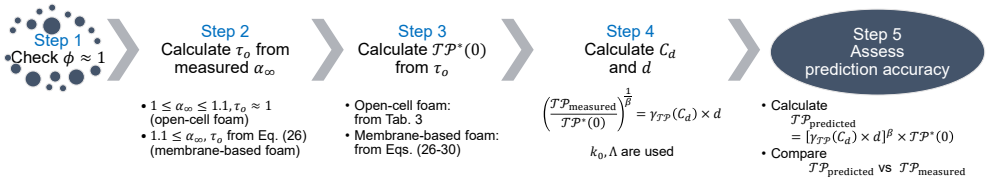

FIG. 7. Schematic representation of the main methodological steps.

The simulation results for the tortuosity α_∞ on random foam structures with membranes are summarized in Eq. (26). These results indicate that the experimental characterization of the tortuosity allows the aperture ratio of membrane τ_o to be accurately determined. This is not surprising since α_∞ is found to be independent from the polydispersity degree C_d (see Sec. III). If $\alpha_\infty \leq 1.1$, the foam is considered to have open cells without any membrane and $\tau_o \approx 1$. In this case, the effect of ligament's cross-section shape might be significant, and therefore the Plateau borders need to be modeled (Fig. 8). Otherwise, when $\alpha_\infty > 1.1$, the situation corresponds to a membrane-based foam, and the ligament's cross-section shape can be neglected from an acoustic point of view. Based on a Kelvin cell with membrane (Fig. 6), Eq. (26) provides an estimate for the aperture ratio τ_o (Step 2, Fig. 7).

The aperture ratio of membrane τ_o determined in Step 2 incorporates transport information $\mathcal{TP}^*(0)$ that can generally be obtained for a monodisperse foam structure ($C_d = 0$) on a periodic cell with an edge length equal to one. At the lowest content of membrane, $\tau_o \approx 1$, and the corresponding dimensionless transport parameters of monodisperse foam $\mathcal{TP}^*(0)$ are given in Tab. III ($0.9 \leq \tau_o \leq 1$). Here, the effect of ligaments cross-section shape might be significant and the Plateau borders are modeled through the Surface Evolver program[45]. Note that the dimensionless transport parameters $\mathcal{TP}^*(0)$ can also be obtained using the approximate formulas in Ref.[38], with a solid volume fraction $\phi_s = 1 - \phi = 0.02$ and an appropriate critical solid volume fraction $\phi_s^* = 0.38$ (for real foam samples). Similar results

are obtained for $0 < \tau_o < 0.9$ in Fig. 6, where results for intermediate membrane content are obtained using Eqs. (26)-(30) (Step 3, Fig. 7).

Analytical calculations of the transport parameters $\mathcal{TP}(C_d)$ on a system having an average pore diameter d and a polydispersity degree C_d are not available. However, the morphological parameters (C_d, d) are contained in the following equation:

$$\left[\frac{\mathcal{TP}_{\text{measured}}}{\mathcal{TP}^*(0)}\right]^{1/\beta} = \gamma_{\mathcal{TP}}(C_d) \times d \ . \tag{34}$$

In principle, any couple of measured transport parameters $\mathcal{TP}_{\text{measured}}$ can then be used to identify (C_d, d), since $\gamma_{\mathcal{TP}}(C_d)$ can be obtained using the relevant equation in Eqs. (20)-(24) (see Fig. 5a). In practice, viscous and inertial parameters k_0 and Λ are used for sound absorbing materials (Step 4, Fig. 7).

Finally, the last step consists in assessing the accuracy of the estimations thus obtained. This validation step can be performed by calculating transport parameters $\mathcal{TP}_{\text{predicted}}$ from (C_d, d,τ_o), using

$$\mathcal{TP}_{\text{predicted}} = [\gamma_{\mathcal{TP}}(C_d) \times d]^{\beta} \times \mathcal{TP}^*(0) \ . \tag{35}$$

The above predictions can be gauged against experimental results and in particular, for the remaining transport parameters Λ' and k_0' that were not used in the inversion process (Step 5, Fig. 7).

B. Illustrative Examples and Discussion

To assess the relevance of the method, we consider a melamine foam and a polyurethane foam with an open porosity $\phi \approx 1$. Macroscopic properties for these materials were already provided elsewhere[46] and are reported in Tab. II. The choice of these independently obtained experimental data is supported by the idea that transport parameters should be, for the sake of reliability and objectivity, characterized whenever possible from direct experimental methods. We briefly summarize here the techniques from which the parameters of interest are obtained: the open porosity ϕ is measured by the Pressure/mass method developed by Y. Salissou and R. Panneton[39]; the static viscous permeability k_0 is determined by a measurement of the pressure drop depending on the volumetric airflow rate as described in ISO 9053-1:2018; the high-frequency tortuosity α_∞ is provided from an ultrasound technique

based on the increase of the time of flight of the air-borne compressional wave between two ultrasound transducers when there is no material and then a material is placed in between them[40,41]; the characteristic lengths Λ and Λ' are also deduced by means of ultrasound measurements[42,47].

TABLE II. Macroscopic parameters for studied foams: Direct characterization from FOAM-X User's Guide; Cylindrical pore[48]; Perrot *el al.* model[35], HP model[10], and proposed method. The values presented in bold correspond to the parameters which can be compared with the experimental data in order to check the accuracy of the model.

Foam	$d\,(\mu m)$	$C_d\,(-)$	$\tau_o\,(-)$	$\phi\,(-)$	$k_0\,(\times 10^{-10} m^2)$	$\alpha_\infty\,(-)$	$\Lambda\,(\mu m)$	$\Lambda'\,(\mu m)$
Melamine								
Direct Charac.	–	–	–	0.99 ± 0.002	16.71 ± 1.78	1.02 ± 0.01	100 ± 10	190 ± 15
Cylinder pore	232	–	–	0.986	9.69	**1.03**	**144**	**250**
Perrot *el al.* model	305	–	–	0.986	16.71	**1.03**	**190**	**329**
Our model	118	0.51	1	1	16.71	1.03	100	**185**
Polyurethane								
Direct Charac.	–	–	–	0.96 ± 0.020	14.49 ± 2.20	1.79 ± 0.03	66 ± 4	286 ± 59
Cylinder pore	220	–	–	0.986	8.71	**1.03**	**137**	**237**
Perrot *el al.* model	284	–	–	0.986	14.49	**1.03**	**177**	**306**
HP model	1092	0	0.35	0.986	14.49	1.79	**101**	**358**
Our model	593	0.38	0.35	1	14.49	1.79	66	**244**

Let us provide an overview of the models that can be used to calculate the morphological parameters of the foam structures under consideration. Consider a porous media saturated by air without membrane. If the pore structure simply consists in a collection of tubes, with circular cross-section shape, the pore diameter can then be estimated from the viscous permeability k_0 and the open-porosity ϕ, using the classical formula for Poiseuille flow[49]:

$$d_T = 2\sqrt{\frac{8k_0}{\phi}}\,. \tag{36}$$

An alternative way to estimate the pore size from k_0 and ϕ (in the case of a monodisperse

open-cell foam) was proposed by Perrot *et al.*[35]:

$$d_K = \sqrt{\frac{k_0}{k_0^*(0)}}\,, \tag{37}$$

where $k_0^*(0)$ is the reference dimensionless viscous permeability simulated on the Kelvin unit cell (see Fig. 8). To test the accuracy of the above estimations, macroscopic transport parameters can be estimated for each predicted pore size and compared with the experimental results. The dimensionless transport parameters are simulated using a Kelvin three-dimensional unit cell with Plateau borders (see Fig. 8), and are summarized in Tab. III.

Note that in 2012, Hoang and Perrot extended the model by Perrot *et al.* by incorporating the membrane effect on the Kelvin unit cell[10]. This Hoang and Perrot (HP) model uses the viscous permeability k_0, the open porosity ϕ, and the average pore size d as input parameters to determine the macroscopic properties of a monodisperse acoustic foam. To estimate the pore size from the known transport parameters, the HP model can be employed as follows. First, the measured tortuosity α_∞ is used to find the aperture ratio of membrane τ_o. Second, the dimensionless transport parameters of reference $\mathcal{TP}^*(0)$ are simulated on the Kelvin unit cell with membrane (Fig. 6), or by using Eqs. (26)–(30). Third, the measured viscous permeability k_0 is used to identify the pore size d_{KM} from the dimensionless permeability $k_0^*(0)$. Therefore, the viscous and thermal characteristic lengths are calculated to verify the accuracy of the estimated pore size and membrane content. When no membrane is present, the HP model reduces to Perrot *et al.* model. This approach is equivalent to our method when $C_d \to 0$.

For any monodispersed-based model, the macroscopic parameters of the studied foams are then calculated by using the scaling rules and the predicted pore diameter :

$$\alpha_\infty = \alpha_\infty^*(0)\,, \tag{38}$$

$$k_0 = d^2 k_0^*(0)\,, \tag{39}$$

$$k_0' = d^2 k_0'^*(0)\,, \tag{40}$$

$$\Lambda = d\Lambda^*(0)\,, \tag{41}$$

$$\Lambda' = d\Lambda'^*(0)\,, \tag{42}$$

where d stands for either d_T, d_K or d_{KM}. The results of calculations from the three different models (d_T, d_K, d_{KM}) are summarized in Tab. II and compared with the approach proposed in this work (Sec. IV A).

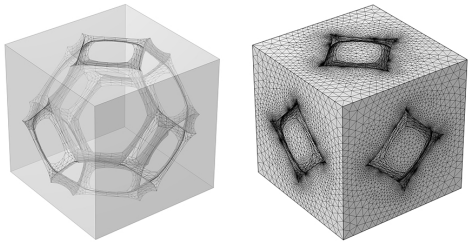

FIG. 8. Kelvin three-dimensional unit cell with Plateau borders.

TABLE III. Dimensionless transport parameters of a monodisperse foam simulated using the Kelvin unit-cell. Here, the porosity ϕ and subsequent calculation of the transport parameters are directly obtained from a geometry derived using the Surface Evolver program.

ϕ	$k_0^*(0)$	$k_0'^*(0)$	$\Lambda^*(0)$	$\Lambda'^*(0)$	$\alpha_\infty^*(0)$
0.986	0.018	0.038	0.623	1.078	1.03

Let us now consider the case of a polydisperse foam. Since both melamine and polyurethane foams exhibit high porosity ($\phi \approx 1$), their membrane content can be estimated using the high-frequency tortuosity α_∞. Indeed, it was shown in Sec. III B 2 that when $\phi \approx 1$, α_∞ only depends on the membrane content τ_o and is independent of the polydispersity C_d. For the melamine foam, $\alpha_\infty \approx 1.05$, which indicates that this foam sample contains no membrane. On the other hand, the polyurethane foam may have substantial membrane content, since $\alpha_\infty = 1.79$. For the melamine foam (now considered as an open-cell foam without membrane content), the dimensionless transport parameters of the reference monodisperse foam without membrane $\mathcal{TP}^*(0)$ are obtained from a Kelvin three-dimensional unit cell (Fig. 8 and Tab. III). For the polyurethane foam, and more generally for any foam with membrane content, the dimensionless transport parameters of the reference monodisperse foam $\mathcal{TP}^*(0)$ depend on the membrane ratio τ_0, which can be estimated from the tortuosity α_∞. Recall that the tortuosity does not depend on pore size polydispersity: $\alpha_\infty^*(0) = \alpha_\infty(C_d)$. From Eq. (26) or Fig. 6b, given the value of the characterized tortuosity $\alpha_\infty = 1.79$ (Tab. II, Polyurethane), it follows that the estimated aperture ratio of the membranes is $\tau_o = 0.35$. The remaining dimensionless parameters of the reference monodisperse foam including membrane content (Fig. 6) can be calculated using Eqs. (26) through (30).

Next, we determine the averaged pore size d and the polydispersity C_d using

$$\left[\frac{k_0}{k_0^*(0)}\right]^{0.5} = \gamma_{k_0}(C_d)\, d\ , \tag{43}$$

$$\frac{\Lambda}{\Lambda^*(0)} = \gamma_{\Lambda}(C_d)\, d\ , \tag{44}$$

where k_0 and Λ are the characterized values given from direct measurements, and C_d and d are the unknowns to be found from the previous set of equations (noticing that $\gamma_{k_0}(C_d)$ and $\gamma_{\Lambda}(C_d)$ are given by Eq. (21) and Eq. (23)). In practice, the ratio of Eqs. (43) and (44) provides the determination of C_d, a value which is then inserted in Eq. (43) or (44) to deduce d. The above steps represent an application of the previously defined methodology to identify, from the experimental knowledge of the transport parameters, the morphological parameters (τ_o, C_d, d). It is worth mentioning that only the visco-inertial transport parameters (k_0, Λ, α_∞) are used to identify these parameters. In addition, using the structure-properties equations describing thermal effects (such as Eqs. (22) and (24)) yields

$$\Lambda' = \left[\gamma_{\Lambda'}(C_d)\, d\right] \Lambda'^*(0)\,, \tag{45}$$

$$k_0' = \left[\gamma_{k_0'}(C_d)\, d\right]^2 k_0'^*(0)\ . \tag{46}$$

We note that the use of Eq. (46) may be limited by the fact that an accurate experimental characterization of k_0' is not routinely available. In this regard, Eq. (45) offers an alternative path since it is usually used, together with the JCA model, to quantify thermal effects[3,4]. Because the morphological parameters were already determined from the visco-inertial structure-property relationships, the remaining thermal structure-property relation (see Eq. (45)) can now be leveraged to provide an estimation of the thermal characteristic length Λ'.

The comparison with experimental results for the melamine foam shows that a simplified model involving either cylindrical pores (Eq. (36) and Eqs. (38)-(42)) or an open-cell foam (Eq. (37) and Eqs. (38)-(42)) provides a correct estimation for the tortuosity α_∞. However, both lead to a significant overestimate of the viscous Λ and thermal Λ' characteristic lengths. Regarding the polyurethane foam, the aforementioned simplified models ignoring membrane effects fail at capturing the experimental values of α_∞, Λ and Λ' all together. In connection with the HP model, we observe that the viscous Λ and thermal Λ' characteristic lengths are overestimated when a model accounting for membrane effects but ignoring polydispersity is

used. The disagreement between the predicted and measured transport parameters suggests that the studied melamine and polyurethane foams are not monodisperse, even with membrane content. Therefore, the corresponding pore diameter d and membrane aperture ratio τ_o obtained by the monodisperse models are geometrical parameters having no connection with the real microstructure.

The polydisperse model including membrane content is expected to be applicable for both fully-open and partially-open foams since it includes the corresponding geometrical features (τ_o, d, C_d). Since the experimental visco-inertial parameters (α_∞, k_0, Λ) were used to identify (τ_o, d, C_d), they cannot be compared with the predictions. However, it is instructive to see that Eq. (45) leads to a thermal characteristic length Λ' in close agreement with the experimental value, for both the melamine and the polyurethane foams.

A few additional comments regarding the pore diameter estimates (using the different models in Tab. II) are relevant at this point. First, a typical range of pore sizes can be extracted from the literature; see the papers by Kino *et al.*[36] and Doutre *et al.*[8] for a polyurethane foams, and Kino *et al.* for melamine foam samples[50]. These data suggest that d lies within the range $[200 - 1600]$ μm for the polyurethane foam, and within $[100 - 300]$ μm for the melamine foam. Based on the microstructural data available in the literature and the comparison between the different existing models, the overall picture emerging from this work is that the predicted pore size distribution from the polydisperse model including membrane content is describing a fairly wide class of disordered foam samples.

Following the remarks in Section III B 2, it is also possible to evaluate the validity of the 3-parameter model of Horoshenkov *et al.*[17,18] for the melamine and polyurethane foams. According to Eqs. (15)–(19), the tortuosity α_∞ can be used to estimate the standard deviation of the pore size σ_d, and each transport parameter can provide a value of the median pore size $\bar{d}$. For the melamine foam, we obtained $\sigma_d \approx 0$, which indicates a monodisperse foam, and the values of $\bar{d}$ obtained from k_0, Λ and Λ' are 232, 200, and 380 μm, respectively. For the polyurethane foam, we found that $\sigma_d = 2.535$ and the values of $\bar{d}$ from k_0, Λ and Λ' were 10425, 909, and 180 μm, respectively. These results show a large discrepancy in the estimation of the median pore size for both types of foams, which confirms that the 3-parameters model is not adequate to describe the considered polydisperse foams (with or without membrane).

Finally, concerning the equivalent pore sizes, it is important to note that the measured

macroscopic parameters of the studied foams satisfy the inequalities in Eqs. (33). Specifically, the equivalent pore sizes are $D_{k_0} = 305 > D_{\Lambda'} = 176 > D_{\Lambda} = 160$ (all in μm) for the melamine foam, while $D_{k_0} = 1092 > D_{\Lambda'} = 872 > D_{\Lambda} = 712$ (all in μm) for the polyurethane foam.

V. CONCLUSION

The main objective of this study was to investigate the impact of pore size polydispersity and membrane content on the acoustic properties of high-porosity solid foam. To achieve this goal, numerical simulations were performed on foam structures generated using Laguerre tessellations, where the pore size distribution was characterized by log-normal probability laws and all membranes were opened by a constant aperture ratio τ_o.

First, the effect of the relative size of the periodic unit cell (PUC) on transport parameters of random foams was studied. In accordance with results reported elsewhere, we found that the size of the PUC required for simulating acoustic properties depends on both the considered transport parameter and level of polydispersity. Results indicate that the viscous permeability k_0 controls the minimum size of the PUC required to reach convergence. Moreover, foams with high polydispersity require a larger number of pores in the PUC to achieve convergence in terms of morphological characteristics — and therefore, on the acoustic properties. This information can help determine the appropriate sample size for experimental characterization and computational modeling of random foam structures.

Second, the influence of pore size polydispersity on the acoustic behavior of solid foams was examined. We analyzed changes in the dimensionless transport parameters $\mathcal{TP}^*(C_d)$, which are normalized with respect to the dimensionless parameters of a foam with a single pore size $\mathcal{TP}^*(0)$. We found that with the same average pore size d and aperture ratio of membranes τ_o, the high-frequency tortuosity α_∞ is almost independent on the size variation of pores, while the pore size polydispersity leads to an increase of the remaining macroscopic parameters. Interestingly, our simulations showed that the ratio $\frac{\mathcal{TP}^*(C_d)}{\mathcal{TP}^*(0)}$ do not depend on the membrane aperture ratio τ_o. Based on this result, we proposed a fast method to predict the acoustic properties of a random foam in a systematic manner, given the dimensionless transport parameters of monodisperse foams. The proposed method also enables the inverse characterization of morphological characteristic of high porous foam from the measured

macroscopic parameters.

ACKNOWLEDGMENTS

This work was supported by the French National Research Agency (ANR-21-PRRD-0001-01) as part of the France Relance project under the Centre National de la Recherche Scientifique research collaborative agreement (REF CNRS number 247060) between CNRS, Université Gustave Eiffel, Université Paris-Est Créteil Val-de-Marne and TREVES, Products, Services and Innovation Group.

DATA AVAILABILITY STATEMENT

The data that support the findings of this study are available from the corresponding author upon reasonable request.

REFERENCES

[1]G. Núñez, R. Venegas, T. G. Zieliński, and F.-X. Bécot, "Equivalent fluid approach to modeling the acoustical properties of polydisperse heterogeneous porous composites," Physics of Fluids **33** (2021), 10.1063/5.0054009, 062008, https://pubs.aip.org/aip/pof/article-pdf/doi/10.1063/5.0054009/15907663/062008_1_online.pdf.

[2]R. Venegas, G. Núñez, C. Boutin, O. Umnova, and Q. Zhang, "Acoustic wave propagation in permeable lossy metamaterials," Physics of Fluids **34**, 017117 (2022).

[3]D. L. Johnson, J. Koplik, and R. Dashen, "Theory of dynamic permeability and tortuosity in fluid-saturated porous media," Journal of Fluid Mechanics **176**, 379–402 (1987).

[4]Y. Champoux and J.-F. Allard, "Dynamic tortuosity and bulk modulus in air-saturated porous media," Journal of Applied Physics **70**, 1975–1979 (1991).

[5]D. Lafarge, P. Lemarinier, J.-F. Allard, and V. Tarnow, "Dynamic compressibility of air in porous structures at audible frequencies," The Journal of the Acoustical Society of America **102**, 1995–2006 (1997).

[6]V. Langlois, C. T. Nguyen, and C. Perrot, "High-frequency permeability of porous media with thin constrictions. II. Porous media containing thin holed membranes," Physics

of Fluids **34** (2022), 10.1063/5.0093672, 077120, https://pubs.aip.org/aip/pof/article-pdf/doi/10.1063/5.0093672/16733855/077120_1_online.pdf.

[7]V. Langlois, "High-frequency permeability of porous media with thin constrictions. I. Wedge-shaped porous media," Physics of Fluids **34** (2022), 10.1063/5.0086257, 077119, https://pubs.aip.org/aip/pof/article-pdf/doi/10.1063/5.0086257/16646521/077119_1_online.pdf.

[8]O. Doutres, N. Atalla, and K. Dong, "Effect of the microstructure closed pore content on the acoustic behavior of polyurethane foams," Journal of Applied Physics **110**, 064901 (2011).

[9]O. Doutres, N. Atalla, and K. Dong, "A semi-phenomenological model to predict the acoustic behavior of fully and partially reticulated polyurethane foams," Journal of Applied Physics **113**, 054901 (2013).

[10]M. Tan Hoang and C. Perrot, "Solid films and transports in cellular foams," Journal of Applied Physics **112**, 054911 (2012).

[11]K. Gao, J. van Dommelen, and M. Geers, "Microstructure characterization and homogenization of acoustic polyurethane foams: Measurements and simulations," International Journal of Solids and Structures **100**, 536–546 (2016).

[12]V. H. Trinh, V. Langlois, J. Guilleminot, C. Perrot, Y. Khidas, and O. Pitois, "Tuning membrane content of sound absorbing cellular foams: Fabrication, experimental evidence and multiscale numerical simulations," Materials & Design **162**, 345–361 (2019).

[13]A. Liebscher and C. Redenbach, "Elastic properties of laguerre approximations of random foams," International Journal of Solids and Structures , 111722 (2022).

[14]S. Aney and A. Rege, "The effect of pore sizes on the elastic behaviour of open-porous cellular materials," Mathematics and Mechanics of Solids **28**, 1624–1634 (2023), https://doi.org/10.1177/10812865221124142.

[15]V. Langlois, C. T. Nguyen, F. Detrez, J. Guilleminot, and C. Perrot, "Permeability of polydisperse solid foams," Phys. Rev. E **105**, 015101 (2022).

[16]S. Föhst, S. Osterroth, F. Arnold, and C. Redenbach, "Influence of geometry modifications on the permeability of open-cell foams," AIChE Journal **68**, e17446 (2022), https://aiche.onlinelibrary.wiley.com/doi/pdf/10.1002/aic.17446.

[17]K. V. Horoshenkov, J.-P. Groby, and O. Dazel, "Asymptotic limits of some models for sound propagation in porous media and the assignment of the pore characteristic lengths,"

The journal of the acoustical society of America **139**, 2463–2474 (2016).

[18]K. V. Horoshenkov, A. Hurrell, and J.-P. Groby, "A three-parameter analytical model for the acoustical properties of porous media," The Journal of the Acoustical Society of America **145**, 2512–2517 (2019).

[19]C. Nguyen, V. Langlois, J. Guilleminot, F. Detrez, A. Duval, M. Bornert, P. Aimedieu, and C. Perrot, "Polydisperse solid foams: Multiscale modeling and simulations of elasto-acoustic properties including thin membrane effects," International Journal of Solids and Structures , 111684 (2022).

[20]R. Quey and L. Renversade, "Optimal polyhedral description of 3D polycrystals: method and application to statistical and synchrotron x-ray diffraction data," Computer Methods in Applied Mechanics and Engineering **330**, 308–333 (2018).

[21]A. M. Kraynik, D. A. Reinelt, and F. van Swol, "Structure of random foam," Physical Review Letters **93**, 208301 (2004).

[22]A. M. Kraynik, D. A. Reinelt, and F. van Swol, "Structure of random monodisperse foam," Physical Review E **67**, 031403 (2003).

[23]J. Koplik, "On the effective medium theory of random linear networks," Journal of Physics C: Solid State Physics **14**, 4821 (1981).

[24]V. Langlois, V. Trinh, C. Lusso, C. Perrot, X. Chateau, Y. Khidas, and O. Pitois, "Permeability of solid foam: Effect of pore connections," Physical Review E **97**, 053111 (2018).

[25]R. J. Brown, "Connection between formation factor for electrical resistivity and fluid-solid coupling factor in Biot's equations for acoustic waves in fluid-filled porous media," Geophysics **45**, 1269–1275 (1980).

[26]M. He, C. Perrot, J. Guilleminot, P. Leroy, and G. Jacqus, "Multiscale prediction of acoustic properties for glass wools: Computational study and experimental validation," The Journal of the Acoustical Society of America **143**, 3283–3299 (2018).

[27]J. H. Park, K. S. Minn, H. R. Lee, S. H. Yang, C. B. Yu, S. Y. Pak, C. S. Oh, Y. S. Song, Y. J. Kang, and J. R. Youn, "Cell openness manipulation of low density polyurethane foam for efficient sound absorption," Journal of Sound and Vibration **406**, 224–236 (2017).

[28]V. Langlois, V. Trinh, and C. Perrot, "Electrical conductivity and tortuosity of solid foam: Effect of pore connections," Physical Review E **100**, 013115 (2019).

[29]P. Mostaghimi, M. J. Blunt, and B. Bijeljic, "Computations of absolute permeability on micro-ct images," Mathematical Geosciences **45**, 103–125 (2013).

[30]T. Kanit, S. Forest, I. Galliet, V. Mounoury, and D. Jeulin, "Determination of the size of the representative volume element for random composites: statistical and numerical approach," International Journal of solids and structures **40**, 3647–3679 (2003).

[31]L. Zhao, H. Li, J. Meng, and D. Zhang, "Efficient uncertainty quantification for permeability of three-dimensional porous media through image analysis and pore-scale simulations," Phys. Rev. E **102**, 023308 (2020).

[32]P. Spanne, J. F. Thovert, C. J. Jacquin, W. B. Lindquist, K. W. Jones, and P. M. Adler, "Synchrotron computed microtomography of porous media: Topology and transports," Phys. Rev. Lett. **73**, 2001–2004 (1994).

[33]J. Skibinski, K. Cwieka, T. Kowalkowski, B. Wysocki, T. Wejrzanowski, and K. J. Kurzydlowski, "The influence of pore size variation on the pressure drop in open-cell foams," Materials & Design **87**, 650–655 (2015).

[34]C. Boutin and C. Geindreau, "Periodic homogenization and consistent estimates of transport parameters through sphere and polyhedron packings in the whole porosity range," Physical review E **82**, 036313 (2010).

[35]C. Perrot, F. Chevillotte, M. Tan Hoang, G. Bonnet, F.-X. Bécot, L. Gautron, and A. Duval, "Microstructure, transport, and acoustic properties of open-cell foam samples: Experiments and three-dimensional numerical simulations," Journal of Applied Physics **111**, 014911 (2012).

[36]N. Kino, G. Nakano, and Y. Suzuki, "Non-acoustical and acoustical properties of reticulated and partially reticulated polyurethane foams," Applied Acoustics **73**, 95–108 (2012).

[37]C. Gaulon, J. Pierre, C. Derec, L. Jaouen, F.-X. Bécot, F. Chevillotte, F. Elias, W. Drenckhan, and V. Leroy, "Acoustic absorption of solid foams with thin membranes," Applied Physics Letters **112**, 261904 (2018), https://pubs.aip.org/aip/apl/article-pdf/doi/10.1063/1.5025407/14513233/261904_1_online.pdf.

[38]V. Langlois, A. Kaddami, O. Pitois, and C. Perrot, "Acoustics of monodisperse open-cell foam: An experimental and numerical parametric study," The Journal of the Acoustical Society of America **148**, 1767–1778 (2020), https://pubs.aip.org/asa/jasa/article-pdf/148/3/1767/14774908/1767_1_online.pdf.

[39]Y. Salissou and R. Panneton, "Pressure/mass method to measure open porosity of porous solids," Journal of Applied Physics **101**, 124913 (2007), https://pubs.aip.org/aip/jap/article-

pdf/doi/10.1063/1.2749486/14998634/124913_1_online.pdf.

[40]J. F. Allard, B. Castagnede, M. Henry, and W. Lauriks, "Evaluation of tortuosity in acoustic porous materials saturated by air," Review of Scientific Instruments **65**, 754–755 (1994), https://pubs.aip.org/aip/rsi/article-pdf/65/3/754/8388186/754_1_online.pdf.

[41]Z. E. A. Fellah, S. Berger, W. Lauriks, C. Depollier, C. Aristégui, and J.-Y. Chapelon, "Measuring the porosity and the tortuosity of porous materials via reflected waves at oblique incidence," The Journal of the Acoustical Society of America **113**, 2424–2433 (2003), https://pubs.aip.org/asa/jasa/article-pdf/113/5/2424/8092531/2424_1_online.pdf.

[42]P. Leclaire, L. Kelders, W. Lauriks, M. Melon, N. Brown, and B. Castagnède, "Determination of the viscous and thermal characteristic lengths of plastic foams by ultrasonic measurements in helium and air," Journal of Applied Physics **80**, 2009–2012 (1996), https://pubs.aip.org/aip/jap/article-pdf/80/4/2009/8052690/2009_1_online.pdf.

[43]R. Panneton and X. Olny, "Acoustical determination of the parameters governing viscous dissipation in porous media," The Journal of the Acoustical Society of America **119**, 2027–2040 (2006).

[44]X. Olny and R. Panneton, "Acoustical determination of the parameters governing thermal dissipation in porous media," The Journal of the Acoustical Society of America **123**, 814–824 (2008).

[45]K. A. Brakke, "The surface evolver," Experimental Mathematics **1**, 141–165 (1992), https://doi.org/10.1080/10586458.1992.10504253.

[46]*FOAM-X 2018 User's Guide*, ESI Group (2018).

[47]J.-P. Groby, E. Ogam, L. De Ryck, N. Sebaa, and W. Lauriks, "Analytical method for the ultrasonic characterization of homogeneous rigid porous materials from transmitted and reflected coefficients," The Journal of the Acoustical Society of America **127**, 764–772 (2010), https://pubs.aip.org/asa/jasa/article-pdf/127/2/764/15292414/764_1_online.pdf.

[48]K. V. Horoshenkov, "A review of acoustical methods for porous material characterisation," Int. J. Acoust. Vib **22**, 92–103 (2017).

[49]H. Darcy, *Les fontaines publiques de la ville de Dijon: exposition et application des principes à suivre et des formules à employer dans les questions de distribution d'eau*, Vol. 1 (Victor dalmont, 1856).

[50]N. Kino, T. Ueno, Y. Suzuki, and H. Makino, "Investigation of non-acoustical parameters of compressed melamine foam materials," Applied Acoustics **70**, 595–604 (2009).